Loss of *DIAPH1* causes SCBMS, combined immunodeficiency, and mitochondrial dysfunction

Meri Kaustio, MSci,[a] Naemeh Nayebzadeh, PhD,[b,c,d] Reetta Hinttala, PhD,[b,c,d] Terhi Tapiainen, MD, PhD,[b,c,d,e] Pirjo Åström, PhD,[f] Katariina Mamia, MSci,[g] Nora Pernaa, MSci,[f] Johanna Lehtonen, MSci,[a,g,h] Virpi Glumoff, PhD,[f] Elisa Rahikkala, MD, PhD,[b,c,i] Minna Honkila, MD, PhD,[b,c,e] Päivi Olsén, MD, PhD,[b,c,e] Antti Hassinen, PhD,[a] Minttu Polso, MSci,[a] Nashat Al Sukaiti, MD,[j] Jalila Al Shekaili, MD, PhD,[k] Mahmood Al Kindi, MD, PhD,[k] Nadia Al Hashmi, MD,[l] Henrikki Almusa, MSci,[a] Daria Bulanova, PhD,[a,m] Emma Haapaniemi, MD, PhD,[g,n,o] Pu Chen, MSci,[a] Maria Suo-Palosaari, MD, PhD,[c,p,q] Päivi Vieira, MD, PhD,[b,c,e] Hannu Tuominen, MD, PhD,[r] Hannaleena Kokkonen, MD, PhD,[c,s] Nabil Al Macki, MD,[t] Huda Al Habsi, MD,[u] Tuija Löppönen, MD, PhD,[v] Heikki Rantala, MD, PhD,[b] Vilja Pietiäinen, PhD,[a] Shen-Ying Zhang, MD, PhD,[w,x,y] Marjo Renko, MD, PhD,[b,v] Timo Hautala, MD, PhD,[f,z] Tariq Al Farsi, MD,[j] Johanna Uusimaa, MD, PhD,[b,c,e*] and Janna Saarela, MD, PhD[a,g,aa,bb*]

Helsinki, Oulu, and Kuopio, Finland; Oslo, Norway; Muscat, Oman; Copenhagen, Denmark; New York, NY; and Paris, France

GRAPHICAL ABSTRACT

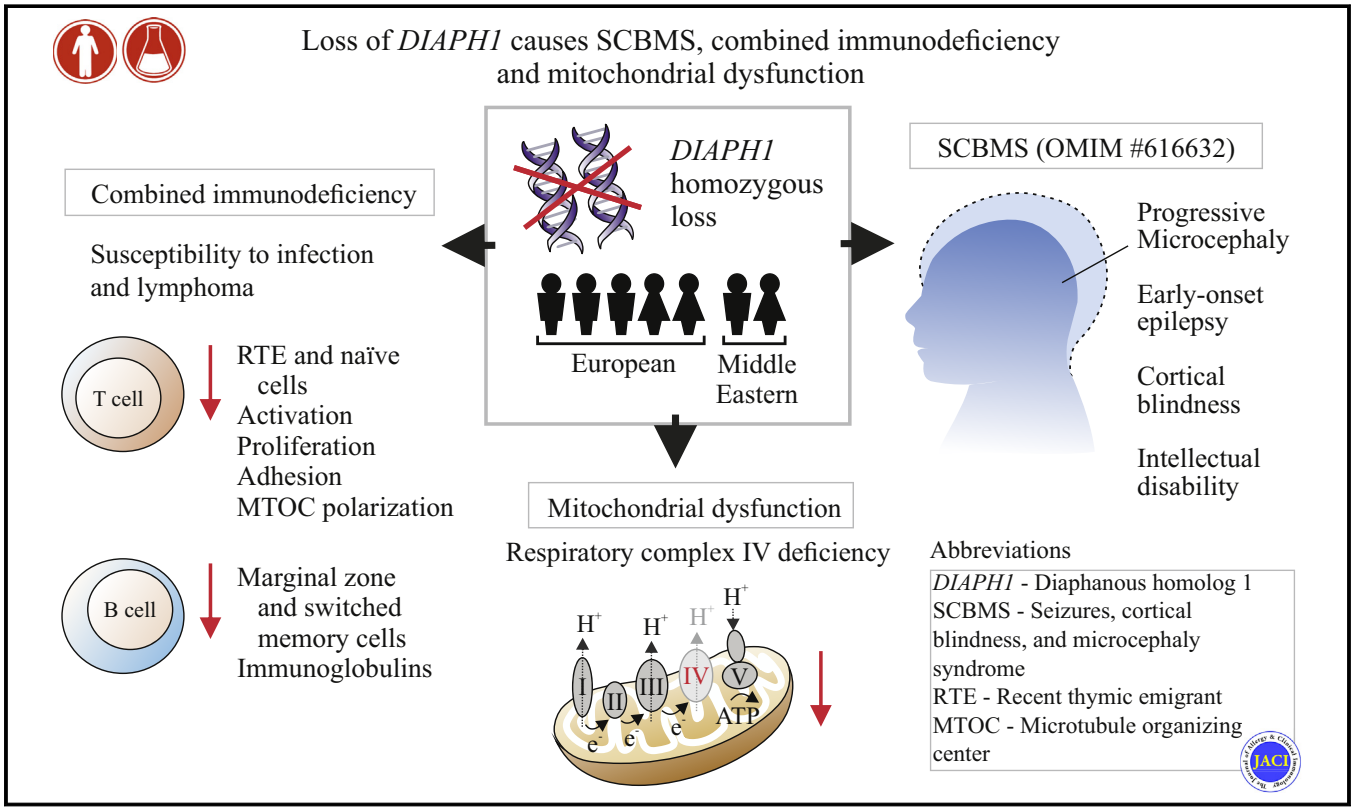

From [a]the Institute for Molecular Medicine Finland (FIMM), HiLIFE, University of Helsinki, Helsinki; [b]PEDEGO Research Unit, University of Oulu, Oulu; [c]the Medical Research Center Oulu, University of Oulu, Oulu; [d]Biocenter Oulu, Oulu; [e]the Department of Pediatrics and Adolescent Medicine, Oulu University Hospital, Oulu; [f]the Research Unit of Biomedicine, University of Oulu, Oulu; [g]the Centre for Molecular Medicine Norway (NCMM), University of Oslo, Oslo; [h]Folkhälsan Research Center, Helsinki; [i]the Department of Clinical Genetics, Oulu University Hospital, Oulu; [j]the Department of Pediatric Allergy and Clinical Immunology, The Royal Hospital, Muscat; [k]the Department of Microbiology and Immunology, Sultan Qaboos University Hospital, Muscat; [l]the Department of Clinical and Biochemical Genetics, The Royal Hospital, Muscat; [m]the Biotech Research and Innovation Centre (BRIC), University of Copenhagen, Copenhagen; [n]the Department of Pediatric Research, Oslo University Hospital, Oslo; [o]the Research Programs Unit, Molecular Neurology and Biomedicum Stem Cell Centre, Faculty of Medicine, University of Helsinki, Helsinki; [p]the Department of Diagnostic Radiology, Oulu University Hospital and University of Oulu; [q]the Research Unit of Medical Imaging, Physics and Technology, Faculty of Medicine, University of Oulu; [r]the Department of Pathology, Oulu University Hospital, Oulu; [s]the Department of Clinical Genetics, Northern Finland Laboratory Centre, Oulu University Hospital, Oulu; the Departments of [t]Pediatric Neurology and [u]General Pediatrics, The Royal Hospital, Muscat; [v]the Department of Pediatrics, University of Eastern Finland and Kuopio University Hospital, Kuopio; [w]St. Giles Laboratory of Human Genetics of Infectious Diseases, Rockefeller Branch, The Rockefeller University, New York; [x]Paris Descartes University, Imagine Institute, Paris; [y]the Laboratory of Human Genetics of Infectious Diseases, Necker Branch, INSERM UMR 1163, Necker Hospital for Sick Children, Paris; [z]the Department of Internal Medicine, Oulu University Hospital, Oulu; [aa]Department of Medical Genetics, Oslo University Hospital, Oslo; and [bb]Department of Clinical Genetics, Helsinki University Hospital, Helsinki.

Background: Homozygous loss of *DIAPH1* results in seizures, cortical blindness, and microcephaly syndrome (SCBMS). We studied 5 Finnish and 2 Omani patients with loss of *DIAPH1* presenting with SCBMS, mitochondrial dysfunction, and immunodeficiency.

Objective: We sought to further characterize phenotypes and disease mechanisms associated with loss of *DIAPH1*.

Methods: Exome sequencing, genotyping and haplotype analysis, B- and T-cell phenotyping, *in vitro* lymphocyte stimulation assays, analyses of mitochondrial function, immunofluorescence staining for cytoskeletal proteins and mitochondria, and CRISPR-Cas9 *DIAPH1* knockout in heathy donor PBMCs were used.

Results: Genetic analyses found all Finnish patients homozygous for a rare *DIAPH1* splice-variant (NM_005219:c.684+1G>A) enriched in the Finnish population, and Omani patients homozygous for a previously described pathogenic *DIAPH1* frameshift-variant (NM_005219:c.2769delT;p.F923fs). In addition to microcephaly, epilepsy, and cortical blindness characteristic to SCBMS, the patients presented with infection susceptibility due to defective lymphocyte maturation and 3 patients developed B-cell lymphoma. Patients' immunophenotype was characterized by poor lymphocyte activation and proliferation, defective B-cell maturation, and lack of naive T cells. CRISPR-Cas9 knockout of *DIAPH1* in PBMCs from healthy donors replicated the T-cell activation defect. Patient-derived peripheral blood T cells exhibited impaired adhesion and inefficient microtubule-organizing center repositioning to the immunologic synapse. The clinical symptoms and laboratory tests also suggested mitochondrial dysfunction. Experiments with immortalized, patient-derived fibroblasts indicated that *DIAPH1* affects the amount of complex IV of the mitochondrial respiratory chain.

Conclusions: Our data demonstrate that individuals with SCBMS can have combined immune deficiency and implicate defective cytoskeletal organization and mitochondrial dysfunction in SCBMS pathogenesis. (J Allergy Clin Immunol 2021;148:599-611.)

Key words: *DIAPH1, SCBMS, microcephaly, mitochondrial dysfunction, T cells, immunodeficiency*

Abbreviations used

CIV: Complex IV
MMP: Mitochondrial membrane potential
MTOC: Microtubule-organizing center
PBL: Peripheral blood lymphocyte
SCBMS: Seizures, cortical blindness, and microcephaly syndrome
WES: Whole-exome sequencing
WT: Wild-type

DIAPH1 encodes for the evolutionarily conserved formin diaphanous homolog 1 (DIAPH1 or mDIA1), which acts downstream of Rho GTPases promoting F-actin polymerization and microtubule stabilization.[1-3] DIAPH1 is composed of an N-terminal regulatory GTPase-binding-diaphanous inhibitory domain followed by a dimerization domain, 2 highly conserved formin homology domains (FH1 and FH2) that orchestrate actin polymerization, and a C-terminal diaphanous autoregulatory domain.[4,5] Cytoskeletal dynamics are relevant for many cellular processes, and hence formins have been implicated in cell morphology, differentiation, adhesion, migration, and proliferation in several cell types.[5] DIAPH1 also participates in regulating mitochondrial trafficking by inducing docking of the mitochondria to the cytoskeleton.[6,7] DIAPH1 has also been implicated in several steps of brain development, including neural migration and neurite formation.[8]

DIAPH1 knockout mice present with ventricular enlargement (brain atrophy) at early and postnatal stages and have marked defects in the function of several types of immune cells.[9-14] DIAPH1 is the predominant isoform of the 3 diaphanous-related proteins (DIAPH1-DIAPH3) in T cells and regulates T-cell function through effects on microtubule-organizing center (MTOC) polarization and actin accumulation at the immunologic synapse.[9,14,15] As a result, $DIAPH1^{-/-}$ mice develop lymphopenia and show defective adherence, migration, chemotaxis, and proliferation of T cells.[9,14] In addition, the aging $DIAPH1^{-/-}$ mice spontaneously develop a myeloproliferative phenotype.[16]

In humans, *DIAPH1* has been implicated in both cancer[17,18] and heritable monogenic disease: Dominant gain-of-function variants in *DIAPH1* cause sensorineural deafness with macrothrombocytopenia (DFNA1),[19-21] whereas homozygous loss of *DIAPH1* causes seizures, cortical blindness, and microcephaly syndrome (SCBMS). In SCBMS, the seizures typically start during the first 6 months of life and are difficult to manage. Head size can be normal at birth, but progressive microcephaly, cortical blindness, and severe intellectual disability soon become evident. Patients can also have difficulty to thrive and have reduced height and weight. In previous studies, some patients suffered bronchiectasis or recurrent respiratory infections, but no clear immunodeficiency or cause for these symptoms was shown.[12,22]

Until now, the SCBMS syndrome has been reported in only 3 consanguineous families, with a total of 9 patients homozygous for damaging *DIAPH1* variants (NM_005219: c.2332C>T; p.Q778X, c.2769delT;p.F923fs, c.3145C>T;p.R1049X).[12,22]

*These authors contributed equally to this study.

This work was supported by the Academy of Finland, Finland (decision nos. RH: 317711, 266498, 273790), Ester and Uuno Kokki Foundation, Finland; the Finnish Cultural Foundation, Finland; The Foundation for Pediatric Research, Finland; the Alma and KA Snellman Foundation, Finland; and Special State Grants for Health Research at the Oulu University Hospital, Finland (grant no. VTR K56772).

Disclosure of potential conflict of interest: The authors declare that they have no relevant conflicts of interest.

Received for publication June 22, 2020; revised November 15, 2020; accepted for publication December 8, 2020.

Available online March 1, 2021.

Corresponding author: Janna Saarela, MD, PhD, PO Box 20, FI-00014, University of Helsinki, Finland. E-mail: janna.saarela@helsinki.fi.

The CrossMark symbol notifies online readers when updates have been made to the article such as errata or minor corrections

0091-6749

https://doi.org/10.1016/j.jaci.2020.12.656

Here, we report 5 Finnish patients homozygous for a previously unpublished pathogenic *DIAPH1* splice-donor variant (c.684+1G>A), as well as 2 additional Omani patients homozygous for the previously described p.F923fs variant. In addition, we extend the clinical and molecular phenotype of SCBMS by showing that patients with SCBMS can present with combined immunodeficiency, lymphoma, and mitochondrial dysfunction, and provide evidence for the role of *DIAPH1* in the function of mitochondria and the human immune system.

METHODS

Sequencing and genomic analyses

DNA and RNA extraction, whole-exome sequencing (WES) and capillary sequencing, genotyping, and data analysis are described in this article's Methods section in the Online Repository at www.jacionline.org. Primers are listed in Table E1 in this article's Online Repository at www.jacionline.org.

Cell isolation and culture

Fibroblast cultures were established from skin biopsies at the Department of Clinical Genetics of Oulu University Central Hospital. Fibroblasts were immortalized by a retroviral vector that expresses the *E7* gene of type 16 human papilloma virus and a retroviral vector that expresses the protein component of human telomerase.[23] PBMCs were isolated from heparin blood using Ficoll-Paque PLUS (GEhealthcare, Chicago, Ill) gradient centrifugation. Peripheral blood lymphocytes (PBLs) were collected after 3- to 16-hour monocyte attachment to culture flasks. Culture media are listed in this article's Methods section in the Online Repository.

Cloning and lentiviral transduction

Full-length human wild-type (WT)-*DIAPH1* cDNA was amplified from control fibroblasts by RT-PCR and ligated into a Gateway-compatible pLXSH-puro lentiviral vector (Invitrogen/ThermoFisher, Waltham Mass). Forty-eight hours after transfection of a Phoenix packaging cell line, lentivirus-containing medium was collected and used in mixture with 4 μg/mL polybrene to transduce fibroblasts as described elsewhere.[24]

Immunophenotyping

Clinical immunophenotyping and T-cell receptor-repertoire analyses were performed by the laboratories of Oulu University Hospital, Helsinki University Hospital, Turku University Hospital, and the Royal Hospital and Sultan Qaboos University Hospital Oman. Phenotyping of IL-17–positive T_H17 cells and regulatory T cells is described in detail elsewhere.[25] T_H1/T_H17-cell cytokine measurements are described in this article's Methods section in the Online Repository. Neutrophil oxidative burst was analyzed with dihydrorhodamine test.

Lymphocyte proliferation assays

Lymphocyte proliferation was measured with 3H-thymidine incorporation (as described elsewhere[26]), EDU incorporation according to manufacturer's recommendations (Invitrogen Click-iT-EdU), or by imaging-based estimation of cell confluence and cell counting (see this article's Methods section in the Online Repository). PBMCs/PBLs were stimulated in the presence of 10 to 20 ng/ml IL-2 (Peprotech, Rocky Hill, NJ) in RPMI media with 10% FBS. Stimulations were performed with PHA (Sigma-Aldrich, St Louis, Mo), concanavalin A, pokeweed mitogens, 1:1 or 1:2 cell-bead ratio of Gibco Dynabeads Human T-Activator CD3/CD28 beads (ThermoFisher, Waltham, Mass), or 1 μg/mL soluble anti-CD3 (OKT3) and anti-CD28 (CD28.2) (Invitrogen) for a maximum of 3 days, after which culture was continued in media with IL-2.

Activation marker analysis

Cells were stimulated as described above, and expression of activation markers analyzed by flow cytometry after 16 to 48 hours. Combinations of the following antibodies were used: BV605-CD3 (#563217), BV421-CD4 (#562425), PE-Cy7-CD8 (#335822), BV786-CD69 (#563834), and PE-CF594-CD25 (#562525) (all from BD Biosciences, Franklin Lakes, NJ) and BV570-CD8 (#301038; BioLegend, San Diego, Calif). DRAQ7 (BD Biosciences) and eFluor 660 (ThermoFisher) were used to gate out dead cells. For DIAPH1 staining, samples were fixed and permeabilized in methanol for 30 minutes, washed, stained for 60 minutes at room temperature for surface markers and rabbit monoclonal DIAPH1 antibody (1:200; ab129167; Abcam, Cambridge, UK), washed, and stained with AF488 goat antirabbit secondary antibody (1:10000; #A11008; Invitrogen). Samples were run on the iQue Screener PLUS flow cytometer and analyzed with ForeCyt software (Sartorius, Goettingen, Germany).

PAGE and western blotting

Blots were probed by the following primary antibodies: SDHA #ab14715, UQCRC2 #ab14745, COX IV #ab14744, ATP5A #ab14748, and DIAPH1 #ab129167 (Abcam); NDUFA9 #A21344 (Life Technologies/ThermoFisher, Waltham, Mass); and GAPDH #258 (ThermoFisher). Secondary detection was performed with Goat Anti-Mouse IgG HRP #1031-05 (SouthernBiotech, Birmingham, Ala), Goat Anti-Rabbit IgG H&L #ab97080 (Abcam) or Swine Anti-rabbit Ig/HRP #P0399 (Dako/Agilent, Santa Clara, Calif), and ECL reagents (Pierce, Appleton, Wis). Total protein was detected with No-stain Protein Labeling Reagent (Invitrogen/ThermoFisher). Imaging was performed with the ChemiDoc MP Imaging System (Bio-Rad, Hercules, Calif), and relative intensity of bands was calculated using Image J software or ImageLab 6.0 (Bio-Rad). Blotting methods are described in more detail in this article's Methods section in the Online Repository.

Immunocytochemistry

Detailed methods for immunofluorescence stainings are described in this article's Methods section in the Online Repository. Briefly, 1- or 10-day cultured T cells were plated on ICAM-1 and CD3 antibody or CD3/CD28 antibody–coated surface, let attach for 1 hour, and fixed with 2% or 4% formaldehyde in PBS. Cells were stained with either (a) Mitotracker Deep Red (#M22426; ThermoFisher; staining of live cells before fixation) or AF647 Phalloidin (#A22287; Invitrogen) and AF555-conjugated α-Tubulin antibody (#MA1-38000-A555; ThermoFisher) and Hoechst 33342 (#14533; Sigma-Aldrich) or (b) CytoPainter Phalloidin iFluor 488 Reagent (#ab176753; Abcam) and Hoechst. Cells were imaged with Olympus FluoView FV1000 confocal microscope or PerkinElmer Opera Phenix high-content confocal microscope at 60× or 63×, respectively. Identical exposure time and offsetting was used for all samples. Images were exported and further analyzed with Harmony 4.9 software in 3D or Fiji.[27] Parameters are listed in Table E2 in this article's Online Repository at www.jacionline.org.

CRISPR-Cas9 knockout of *DIAPH1* in healthy donor PBMCs

DIAPH1 Alt-R CRISPR-Cas9 crRNA guides (listed in Table E1; IDT) were combined 1:1 with Alt-R CRISPR-Cas9 tracrRNA (IDT, 1072533), annealed at 95°C for 5 minutes, and cooled to room temperature. RNPs were produced by complexing 2 *DIAPH1* guides (guide 1 + 2 or guide 1 + 3, each at 100 pmol/sample) with Alt-R S.p. Cas9 Nuclease V3 (IDT; 1081059; 100 pmol) and incubated at room temperature for 15 minutes. Healthy donor PBMCs were stimulated in complete RPMI media with ImmunoCult Human CD3/CD28 T Cell Activator (STEMCELL Technologies, Vancouver, British Columbia, Canada) and 3 ng/mL IL-7 and IL-15 (Peprotech) for 3 days. Cells were resuspended at 1 million cells/20 μL 1 mol electroporation buffer and electroporated using Lonza 4D Nucleofector X unit (Lonza, AAF-1002X), electroporation program "EO-115," and "Primary-Cell-P3" solution. After

TABLE I. Summary of phenotypic characteristics of the studied patients

	Patient						
Characteristic	**F1.P1**	**F1.P2**	**F2.P3**	**F3.P4**	**F4.P5**	**F5.P6**	**F5.P7**
Age (y)		—	7	3		—	3
Age of death (y)	9	6	—	—	29	3	—
Sex	Male	Male	Male	Female	Female	Female	Male
Cause of death	B-cell lymphoma	Status epilepticus	—	—	Pneumonia, encephalitis	B-cell lymphoma	—
Microcephaly	Progressive (from −2.5 SD at 1.5 y to −5.5 SD)	Progressive (from −1.0 SD at birth to −5.5 SD)	Progressive (from −3.7 SD at birth to −7.6 SD at 4 y 5 mo)	Progressive (from −1.4 SD at birth to −6.3 SD at 2 y 1 mo)	Progressive	Progressive (from −2.0 SD at 10 wk to −4.8 SD at 3 y 2 mo)	Progressive (from fourth percentile at 3 wk to −4.5 SD at 3 y)
Brain imaging	Abnormal signal intensities in occipital white matters; thin chiasm and optic nerves	Abnormal signal intensities in occipital white matter; thin chiasm and optic nerves	Abnormal signal intensities in occipital white matter; thin chiasm and optic nerves	Normal at the age of 5 d	Occipital atrophy at age 27 y, encephalitis at age 29 y	Brain atrophy	Partial agenesis of corpus callosum, occipital atrophy
Intellectual disability	Profound	Profound	Profound	Profound	Profound	Profound	Profound
Epilepsy onset	2 mo	2 mo	2.5 mo	2 d	1 mo	2 mo	15 d
Visual impairment	Cortical blindness	Cortical blindness	Cortical blindness	Cortical blindness	Cortical and optic nerve athrophy	Cortical blindness and optic nerve atrophy	Cortical blindness
Muscles	Muscular atrophy, increased fat and number of mitochondria	Muscular atrophy, increased fat and number of mitochondria	Mild muscular hypotonia, muscle biopsy not taken	Normal muscle tone, muscle biopsy not taken	Normal muscle tone, muscle biopsy not taken	Muscular hypotonia, muscle biopsy not taken	Mild muscular hypotonia, muscle biopsy not taken
Severe/ recurrent infections	Bacterial otitis media, *candida*, mycobacteria, VZV, HSV, EBV, *Molluscum contagiosum*	Respiratory infections, *Molluscum contagiosum*	Otitis media and respiratory infections	Recurrent watery diarrhea, respiratory infections	Rubella vaccine strain skin infection, JCV encephalitis	*Candida*, *Staphylococcus haemolyticus, Elizabethkingina meningoseptica*, EBV, CMV	Otitis media, *Streptococcus pneumonia*, MRSA, RSV bronchiolitis
Lymphoma (B cell)	Diffuse large B-cell lymphoma	Hodgkin-like (detected in autopsy)	No	No	No	Diffuse large B-cell lymphoma	No

CMV, Cytomegalovirus; *HSV*, herpes simplex virus; *JCV*, John Cunningham virus; *MRSA*, methicillin-resistant *Staphylococcus aureus*; *RSV*, respiratory syncytial virus; *VZV*, varicella-zoster virus.

electroporation, 80 μL/sample of RPMI with 10% FBS and IL-2 at 500 U/mL was added and cells were allowed to rest at 37°C for 15 minutes, followed by transfer into 24-well plate in 400 μL medium. Cells were since cultured at a concentration of 0.5 to 2 × 10^6/mL. Five days after electroporation, cells were restimulated either as before electroporation or with 1:2 ratio of CD3/CD28 beads (ThermoFisher). After 16 and 40 hours, cells were collected for activation marker analysis by flow cytometry.

Statistics and data visualization

Welch *t* test (fluorescence intensity) and Student *t* test (western blot band intensities, imaging data) were used to calculate *P* values between groups. Data were handled and plotted with R (4.0.3) using the ggplot2 package in Rstudio (v1.3.1093).[28,29]

Study approval

This study was approved by the Regional Ethics Committee of the Northern Ostrobothnia and the Research and Ethics Review and Approval Committee in Ministry of Health, Oman, and conducted according to the principles of the Helsinki Declaration. Written informed consents were obtained from caregivers of the patients, their family members, and healthy controls.

RESULTS

Identification of patients with *DIAPH1*-related disease

We studied 7 patients with SCBMS originating from Finland and Oman, who presented with a global developmental delay with progressive microcephaly, drug-resistant early-onset epileptic seizures, cortical blindness, and deficiency of cellular immunity (Table I). To identify a genetic cause for the disease, we acquired WES of all patients. WES data were analyzed for rare (frequency <0.01), exonic or splice region variants that followed either X-chromosomal–recessive, autosomal-recessive, or compound heterozygous inheritance, as well as for *de novo* variants. WES identified a homozygous splice-donor variant in *DIAPH1* (chr5:140961878, C>T; rs766545876; NM_005219:c.684+1G>A) in all Finnish patients, although the families were not known to share recent ancestry. The variant was validated by targeted capillary sequencing (see Fig E1 in this article's Online Repository at www.jacionline.org). In the 2 Omani patients, diagnostic WES analyses found a homozygous, previously published pathogenic NM_005219:c.2769delT;p.F923fs variant (Fig 1, *A* and *B*).[22] No other

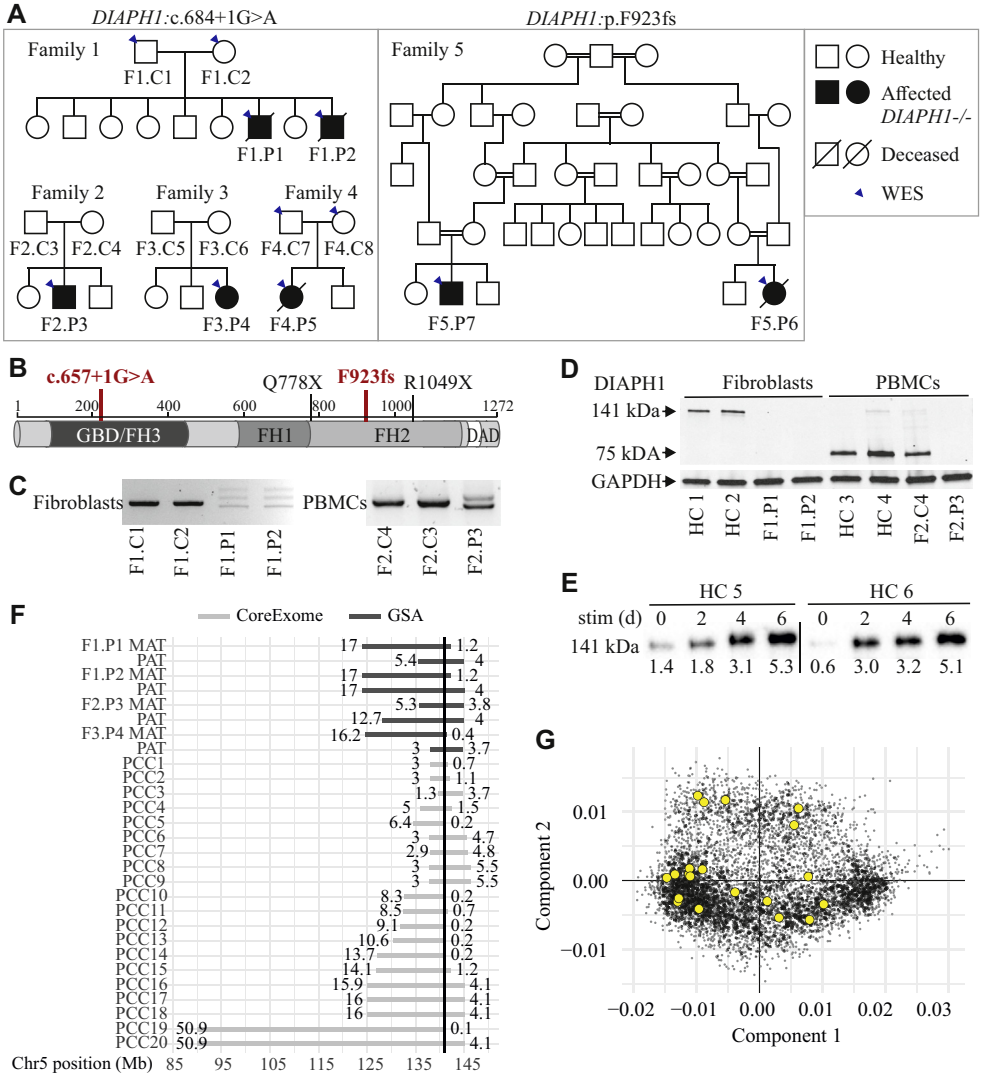

FIG 1. Genetics and effects of *DIAPH1* variants. **A,** Pedigrees of studied families. For F1, only those siblings who participated in segregation analysis are displayed. **B,** DIAPH1 protein structure showing published SCBMS-causing variants. Variants found in patients in this article are marked in red. **C,** Gel separation of PCR amplicons spanning the variant from patient-derived and parental cDNA. **D,** Total protein from patient and healthy control–derived fibroblasts or PBMCs was run on SDS-PAGE gel, blotted, and probed for DIAPH1. GAPDH was used as a loading control. **E,** Total protein from PBL of 2 healthy controls was collected every 2 days since stimulation (stim) by anti-CD3/CD28, blotted, and probed for DIAPH1. Numbers below bands indicate relative band volume intensity after total protein normalization, with the average of the 0-day samples set to 1. Black line indicates samples were run on the same gel but were noncontiguous. **F,** Lengths of shared haplotype segments around the c.684+1G>A variant in phased array data. Data from patients (GSA-chip) are shown as dark gray bars, and data from heterozygous carriers (PCC1-20, CoreExome-chip) are shown as light gray bars. Numbers next to bars represent haplotype arm lengths around the variant (black vertical line) in megabases (Mb). **G,** MDS plot (first 2 dimensions) was constructed to visualize genetic distances between 20 variant carriers in a Finnish population cohort. Gray dots: noncarrier, yellow dots: *DIAPH1* c.684+1G>A heterozygote. *GAPDH*, Glyceraldehyde-3-phosphate dehydrogenase; *HC*, healthy control; *MAT*, maternal haplotype; *MDS*, multidimensional scaling; *PAT*, paternal haplotype.

pathogenic variants were identified. Other variants surviving filtering in families 1, 4, and 5 are listed in Table E3 in this article's Online Repository at www.jacionline.org.

Analysis of patient-derived cDNA showed that the c.684+1G>A variant resulted in aberrant splicing of *DIAPH1* (Fig 1, *C*; see Fig E2 and capillary sequencing results in this article's Online Repository at www.jacionline.org). Only WT transcript was detected in heterozygotes, possibly due to dosage compensation and preferential PCR amplification of the more abundant WT transcript. Western blot of immortalized fibroblast and PBMC total protein extracts indicated total loss of the DIAPH1 protein in patients (Fig 1, *D*). In control fibroblasts, only the 141-kDa full-length DIAPH1 was detected, whereas unstimulated control PBMCs contained very little of the full-length protein and higher amounts of a shorter isoform of approximately 75 kDa.[15] In healthy donor PBMCs in response

TABLE II. Immunophenotype of patients with SCBMS

Parameter	Patient							Reference values
	F1.P1	F1.P2	F2.P3	F3.P4	F4.P5	F5.P6	F5.P7	
Age at sampling (y)	9	4	7	3	25	3	3	
Leukocytes	8.0	11.0	9.5	13.4	6.0	NA	NA	4.5-13.5 × 10^9
Neutrophils	4.8	4.1	6.2	7.1	4.8	0.7 ↓	2.6	4.5-13.5 × 10^9
Lymphocytes	2.1	5.1	1.4	4.6	1.0 ↓	0.48 ↓	4.6	1.2-3.5 × 10^9
$CD19^+$ B cells	437	765	342	1597	312	1% ↓	760	a: 80-616 / 17%-26%
Transitional $CD38^{hi}IgM^{hi}$	NA	NA	11.1% ↑	19.1% ↑	6.3%↑	Low↓	11% ↑	a: 0.6%-3.5%
Naive $CD27^-IgD^+IgM^+$	NA	NA	89.8% ↑	94.6%	72.2%	Low↓	82%	a: 43.2%-82.4%
Memory $CD27^+$	NA	NA	8.2%↓	4.4%↓	1.5%↓	Low↓	5%↓	
Marginal zone $CD27^+IgD^+IgM^+$	NA	NA	4.2% ↓	2.2% ↓	0.5% ↓	Low↓	6% ↓	a: 7.2%-30.8%
Switched memory $CD27^+IgD^-IgM^-$	NA	NA	2.6% ↓	1.6% ↓	0.7% ↓	Low↓	5% ↓	a: 6.5%-29.2%
Plasmablasts $CD38^{++}IgM^-$	NA	NA	<0.2%	<0.2%	<0.2%	Low	1%	a: 0.4%-3.6%
Activated $CD38^{low}CD21^{low}$	NA	NA	3.8%	4.2%	6.9%	Low↓	4%	a: 0.8%-7.7%
$CD3^+$ T cells	2100	3315	729 ↓	2512	453 ↓	470 ↓	2970	a: 742-2750 / 56%-86%
$CD4^+$	582	1122	483	1039	189 ↓	50 ↓	510	a: 404-1612 / 33%-58%
$CD8^+$	624	1785	300	1140	272	440	2210	a: 220-1129 / 13%-39%
CD4/CD8	0.93	0.63	1.6	0.9	0.7	0.11	0.23	a: 0.6-2.8
NK	624	21%	466	507	105	70	680	a: 84-724 / 5%-26%
RTE $CD45RA^+CD62L^+CD31^+$	NA	NA	1.4% ↓	1.2% ↓	0.5% ↓	1% ↓	9% ↓	a: 14.4%-38.3%
$CD4^+CD3^+$ T cells								
Naive ($CD45RA^+CCR7^+$)	NA	NA	4.4% ↓	4.4% ↓	4.9% ↓	1% ↓	5% ↓	a: 20.5%-54.8%
TCM ($CD45RA^-CCR7^+$)	NA	NA	28.0%	19.5%	47.2%	20%	40%	a: 8.4%-32.8%
TEM ($CD45RA^-CCR7^-$)	NA	NA	61.9%	56.8%	46.0%	77%	53%	a: 19.9%-52.4%
TEMRA ($CD45RA^+CCR7^-$)	NA	NA	5.7%	19.2%	2.0%	2%	3%	a: 1.4%-17.0%
Treg $FOXP3^+CD25^+$	NA	NA	3.8%	1.0%	4.2%	NA	NA	HC: 2.0%-4.1%
Treg $CD127^-CD25^+$	NA	NA	4.7%	1.5%	4.3%	NA	NA	HC: 3.2%-5.7%
Treg *in vitro* suppression	NA	NA	NA	NA	Normal	NA	NA	
T_H17: IL-17A in $CD69^+$, CD3/CD28-stimulated cells	NA	NA	6.9%	2.3%	6.4%	NA	NA	HC: 0.8%-1.4%
T_H17: IL-17A in PMA-stimulated cells	NA	NA	2.4%	1.3%	4.6%	NA	NA	HC: 0.2%-0.7%
T_H1: IFN-γ in PMA-stimulated cells	NA	NA	46.3%	42.3%	38.1%	NA	NA	HC:16.2%-17.7%
$CD8^+CD3^+$ T cells								
Naive ($CD45RA^+CCR7^+$)	NA	NA	2.5 ↓	1.6 ↓	6.9 ↓	1 ↓	1 ↓	a: 18.8%-71.0%
TCM ($CD45RA^-CCR7^+$)	NA	NA	0.8	0.4	16.3	1	2	a: 1.2%-7.3%
TEM ($CD45RA^-CCR7^-$)	NA	NA	18.9	10.7	31.2	75	61	a: 14.6%-63.0%
TEMRA ($CD45RA^+CCR7^-$)	NA	NA	87.8	39.0	45.5	24	36	a: 4.5%-33.7%
TCR repertoire (TCRG)	NA	Oligoclonal pattern	Weak clonal expansion*	Weak clonal expansion*	Weak clonal expansion*	Oligoclonal pattern	Oligoclonal pattern	
Immunoglobulins								
S-IgG	11.9	10.58	9.0	7.1	3.1↓	7.0	11.8	a: 6.77-15; 0-4 y: 2.3-13.1
S-IgA	0.96	2.34↑	1.94	0.29	0.66↓	0.58↓	1.24	a: 0.88-4.84; 0-4 y: 0.1-1.8
S-IgM	0.18↓	0.55↓	0.63 ↓	1.04	<0.1↓	4.02	1.3	a: 0.88-4.84; 0-4 y: 0.2-1.9
S-IgE	<5	<5	184	NA	<2	NA	734	0-130
Vaccine responses								
Pneumovax	NA	NA	NA	NA	Absent	Normal	Normal	
Tetanus	NA	NA	Normal	Normal	Normal	Normal	Normal	
Neutrophil function								
Oxidative burst	NA	NA	Normal	Normal	Normal	NA	NA	
Complement								
CH50, CH100	Normal	Normal	Normal	Normal	Normal	NA	NA	
C3, C4	NA	NA	NA	NA	Normal	Normal	NA	
Lymphocyte stimulation responses								
Pokeweed mitogens	NA	NA	Weak	Weak	Very weak	NA	NA	
PHA	NA	NA	Weak	Absent	Weak	Absent	Very weak	
Concanavalin A	NA	NA	Very weak	NA	Very weak	NA	NA	

(Continued)

TABLE II. *(Continued)*

Parameter	Patient							Reference values
	F1.P1	F1.P2	F2.P3	F3.P4	F4.P5	F5.P6	F5.P7	
Anti-CD3 + anti-CD28, beads	NA	NA	Very weak	Absent	Very weak	NA	NA	
Anti-CD3 + anti-CD28, soluble	NA	NA	Normal	Absent	Normal	NA	NA	

a, Adults; *NA*, not applicable/available; *RTE*, recent thymic emigrant; *TCR*, T-cell receptor.
Absolute lymphocyte counts for F1.P2. were not available.
*The clinical significance of the observed 1-3 clonal expansions is not known, and may be reactive.

to stimulation with soluble anti-CD3/CD28 or with PHA, the amount of full-length DIAPH1 increased, suggesting that DIAPH1 is relevant for proliferating lymphocytes (Fig 1, *E*; see Fig E3 in this article's Online Repository at www.jacionline.org).

The novel *DIAPH1*:c.684+1G>A disease variant is enriched in the Finnish population

Comparison of variant frequency between populations in the Genome Aggregation Database[30] revealed that the c.684+1G>A variant is enriched in the Finnish population at an allele frequency of 0.001125. In genotype data from approximately 11,400 individuals from Finnish population cohorts (FINRISK and TWIN studies),[31,32] the variant was present at a similar allele frequency. To investigate whether the c.684+1G>A variant had arisen from a single mutational event, we carried out haplotype analysis for 20 unrelated, heterozygous, variant carriers in the cohort. The analysis indicated that the c.684+1G>A variant lied on a shared ancestral haplotype with a median length of 8.8 Mb for shared haplotype segments (Fig 1 *F*; see Tables E4 and E5 in this article's Online Repository at www.jacionline.org). Average pairwise identity-by-descent-sharing coefficients (PI-HAT) were 0.0038 for the whole cohort and 0.0067 for variant carriers, with values ranging from 0 to 0.03 between distinct patient sample pairs (see Table E6 in this article's Online Repository at www.jacionline.org), indicating greater than average genomic sharing between some but not all carriers. Similarly, on a multidimensional scaling plot, some of the variant carriers clustered together whereas others exhibited comparatively low genomic sharing (Fig 1, *G*). This suggests that the mutational event has not taken place very recently. Using a previously published approach[33] that uses the information on the haplotype arm lengths and assuming a correlated genealogy, the age of the mutation was estimated at 17.9 generations (95% CI from 4.3 to 32.5 generations).

Clinical characteristics of patients with SCBMS

Detailed clinical descriptions for each patient can be found in this article's Online Repository at www.jacionline.org. Shortly, all studied patients had microcephaly, developmental delay, epilepsy, and cortical blindness characteristic to the SCBMS syndrome (Table I). Brain magnetic resonance imaging of patients F1.P1, F1.P2, and F2.P3 demonstrated thin chiasm and optic nerves, and T2-hyperintense white matter and cortical signal abnormalities in bilateral occipital lobes (see Fig E4, *A*, in this article's Online Repository at www.jacionline.org). The clinical presentation of F4.P5 and brain magnetic resonance imaging have been previously described.[34] In autopsy, neuropathological examination of F1.P2 and immunohistochemical stainings revealed several morphological abnormalities (Fig E4, *B* and *C*). In family 1, mitochondrial disease was suspected on the basis of progressive brain atrophy, mildly elevated lactate/puryvate ratio in blood, and increased number of mitochondria and mild increase in fat in muscle biopsies. F2.P3, F5.P6, and F5.P7 also presented with muscular hypotonia. Moreover, the patients showed signs of immunodeficiency. F1.P1 and F1.P2 suffered recurrent respiratory infections as well as persistent and extensive *Molluscum contagiosum* lesions. In addition, F1.P1 had recurrent oral *herpes simplex* virus and fungal infections throughout his childhood. At 19 years, he had EBV viremia and subsequently developed and succumbed to diffuse large B-cell lymphoma. F1.P2 died of nonimmune causes (status epilepticus) at the age of 6 years, but autopsy revealed a subclinical Hodgkin-type lymphoma. In addition, patient F5.P6 died of EBV-positive B-cell lymphoma at age 3 years (see Fig E5 in this article's Online Repository at www.jacionline.org). Patient F4.P5 suffered from persistent vaccine strain Rubella skin infection and progressive multifocal leukoencephalopathy positive for John Cunningham virus. These clinical findings are consistent with poor T-cell immunity.

B-cell maturation defects

Complement activity, natural killer cell, and neutrophil counts and oxidative burst were normal in all tested patients. However, 5 of the 7 patients were deficient with at least 1 major immunoglobulin class. $CD19^+$ B cells were very low in 1 patient (F5.P6), and immunophenotyping showed that proportions of memory B cells, marginal zone $CD27^+IgD^+IgM^+$, and switched memory $CD27^+IgD^-IgM^-$ B cells were low in the other 4 patients from whom PBMCs were available for analysis (Table II). Proportions of transitional $CD38^{hi}IgM^{hi}$ B cells in turn were elevated.

DIAPH1 is required for T-cell function

Lymphocyte differentials indicated abnormalities in the T-cell compartment: $CD3^+$ T-cell counts were low or normal and showed skewing of the CD4/CD8 ratio below 1. Patients consistently showed defective T-cell maturation with low naive $CD4^+CD3^+$ and $CD8^+CD3^+$ (CD45RA+CCR7+) T-cell populations and nearly absent $CD45RA^+CD62L^+CD31^+$ recent thymic emigrant cells. Proportion of IFN-γ and IL-17–positive $CD4^+$ T-cell counts were high, indicating T_H1 and T_H17 activity, respectively.

All patients from whom PBMCs were available for analysis repeatedly showed a poor or absent lymphocyte proliferation response to stimulation by concanavalin A, PHA, or anti-CD3/CD28–coated beads (Table II; Fig 2, *A* and *B*). However, responses to soluble antibodies or pokeweed mitogens varied

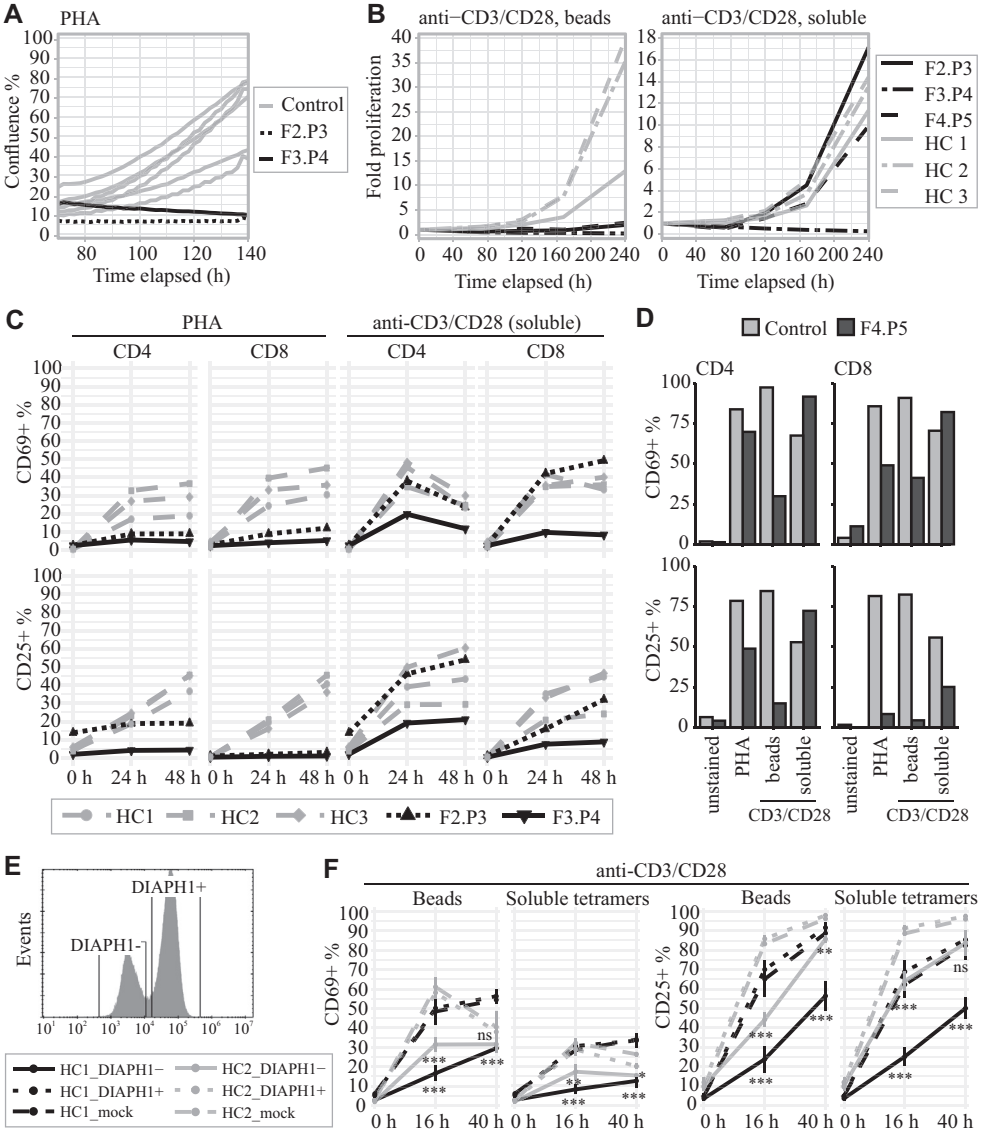

FIG 2. DIAPH1 is required for optimal T-cell responses. (**A**) PBL proliferation after stimulation by PHA was estimated by phase-contrast imaging on ICAM-1–coated wells and (**B**) after stimulation by either anti-CD3/CD28–coated beads (1:2 cell-bead ratio) or a mix of soluble anti-CD3/CD28 tetramers, IL-7 and IL-15 (both 3 ng/mL), by counting fold cell proliferation. **C** and **D,** Upregulation of activation markers CD69 and CD25 in response to PHA or soluble antibodies or bead-bound anti-CD3/CD28 was assessed as a percentage of $CD3^+CD4^+$ and $CD3^+CD8^+$ T cells by flow cytometry in patients F2.P3 and F3.P4 (Fig 2, *C*) and F4.P5 (Fig 2, *D*). **E,** Example of gating of $DIAPH1^-$ and $DIAPH1^+$ T cells in flow cytometry data after *DIAPH1* knockout from healthy control PBMCs by CRISPR-Cas9. **F,** Transfected and mock-electroporated cells were stimulated with either anti-CD3/CD28–coated beads or a soluble anti-CD3/CD28 tetramer with IL-7 and IL15, and upregulation of CD69 and CD25 was assessed by flow cytometry. Results were pooled from duplicate samples generated with 2 different guide-pairs (N = 4 per data point). *HC,* Healthy control; *ns*, not significant. $*P < .5$, $**P < .01$, $***P < .001$ (Student *t* test for 4 replicates assuming unequal variances).

from normal to absent between patients. Similarly, in flow cytometric analysis after *in vitro* stimulation with PHA or anti-CD3/CD28 beads, patient-derived T cells exhibited poor upregulation of the activation markers CD69 and CD25, especially in the $CD8^+$-cell subset (Fig 2, *C* and *D*). Stimulation with soluble anti-CD3/CD28 resulted in a more variable result: poor upregulation of both markers in F3.P4, otherwise normal response except for weak CD25 upregulation in $CD8^+$ T cells in F4.P5, and a WT-like response in F2.P3. Of note, F2.P3 showed high spontaneous lymphocyte activation similar to what is sometimes seen with chronic herpes simplex virus infection, but test results for herpes simplex virus and EBV were negative.

To confirm reduced proliferation instead of increased apoptosis of activated lymphocytes, the percentage of apoptotic cells was estimated in 2 patients via an imaging-based AnnexinV-binding assay. Neither patient showed increased activation-induced cell death after stimulation by PHA or anti-CD3/CD28, although baseline percentage of AnnexinV-positive cells was higher in the F2.P3 sample than in controls (see Fig E6 in this article's Online Repository at www.jacionline.org).

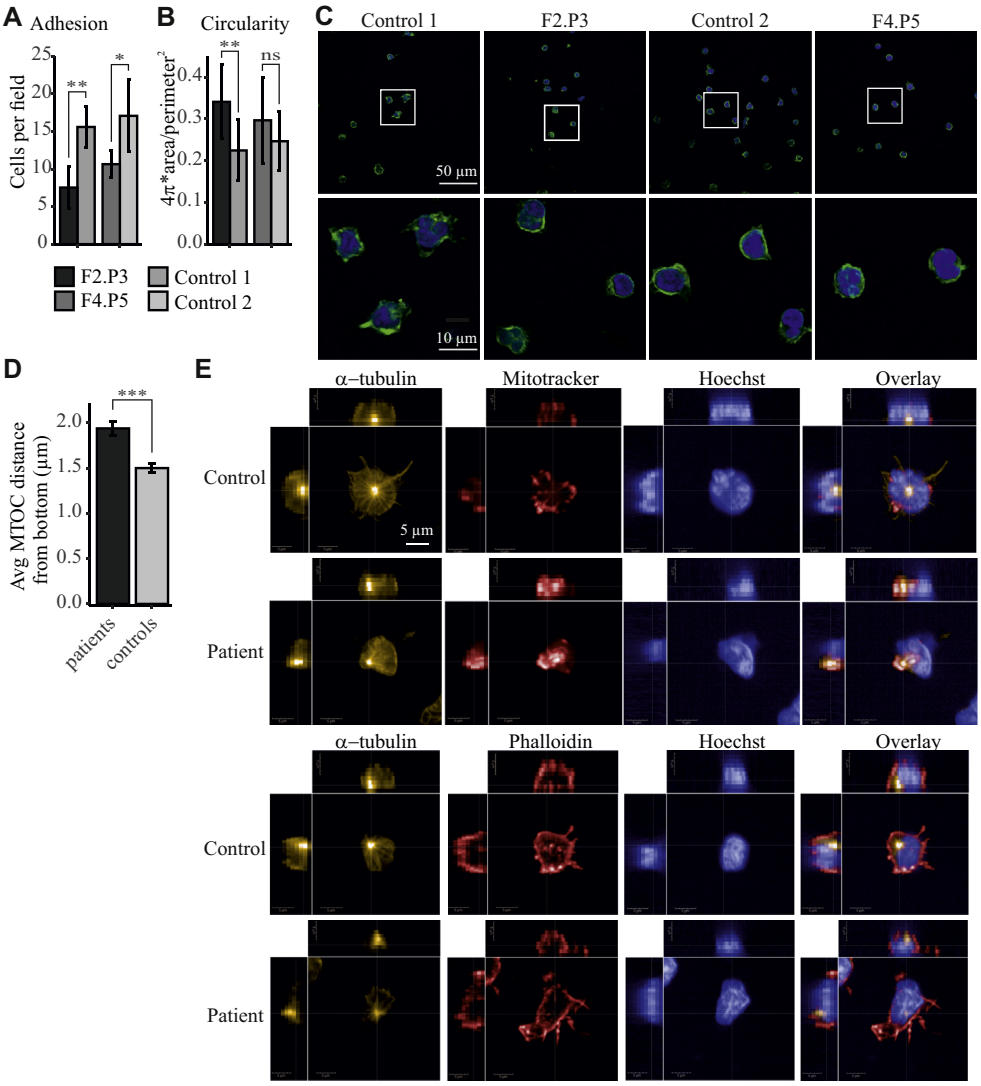

FIG 3. Analysis of T-cell adhesion, shape, and cytoskeletal organization. **A-C,** A total of 25,000 T cells were plated on 8-well chamber slide coated with CD3 and CD28 antibodies, let attach for 1 hour, fixed, and stained for F-actin. Imaging was done with Olympus FluoView FV1000 confocal microscope at 60×. *A,* The number of adhered cells counted from 6 replicate wells (~3-7 images/well) was lower for patient samples than for healthy controls ($P = .001$ for F2.P3/control; $P = .016$ for F4.P5/control II). *B,* Cell circularity index (where 1 = perfect circle) of 12 to 17 cells per study subject was measured using Fiji image analysis software. The circularity index was higher in patient cells compared with control cells although only significantly so for F2.P3 ($P = .003$). Error bars = SD. **C,** Representative microscopic fields of patient and control cells. Blue = Hoechst (nucleus), green = Phalloidin (F-actin). **D,** T cells from 3 healthy donors and 2 patients (F2.P3 and F4.P5) were stained for α-tubulin to visualize the MTOC. The MTOC distance from ICAM-1 + anti-CD3–coated surface was measured in 3D in 300 cells/sample with Harmony 4.9 software, and average distances were compared between patients and controls. Error bars = SD of the mean. **E,** Representative microscopic fields of patient and control cells. Yellow = α-tubulin (MTOC), Red (upper panel) = MitoTracker Deep Red (mitochondria), Red (lower panel) = Phalloidin AF647 (F-actin), Blue = Hoechst (nucleus). Student *t* test: $*P < .05$, $**P < .01$, $***P < .001$.

Knockout of *DIAPH1* in healthy donor PBMCs replicates the SCBMS patient T-cell phenotype

To confirm that the T-cell activation defect was due to lack of *DIAPH1*, we generated *DIAPH1* knockout cells from PBMCs of 2 healthy donors with the CRISPR-Cas9 method. Seven days after electroporation, 20% to 40% of cells in each replicate sample were negative for DIAPH1 protein ($DIAPH1^-$) as estimated by flow cytometry (Fig 2, *E*). Samples were stimulated with anti-CD3/CD28 beads or soluble antibody tetramers to assay upregulation of activation markers and proliferation. At 16 and 40 hours after stimulation, the percentage of cells positive for CD69 and CD25 was markedly reduced in $DIAPH1^-$ cells compared with $DIAPH1^+$ cells from the same donor (Fig 2, *F*). In addition, after gating of CD69- or CD25-positive cells, median fluorescence intensities of CD69 and CD25, respectively, were significantly lower for $DIAPH1^-$ cells at most time points (see Fig E7 in this article's Online Repository at www.jacionline.org). Hence, knockout of *DIAPH1* in healthy

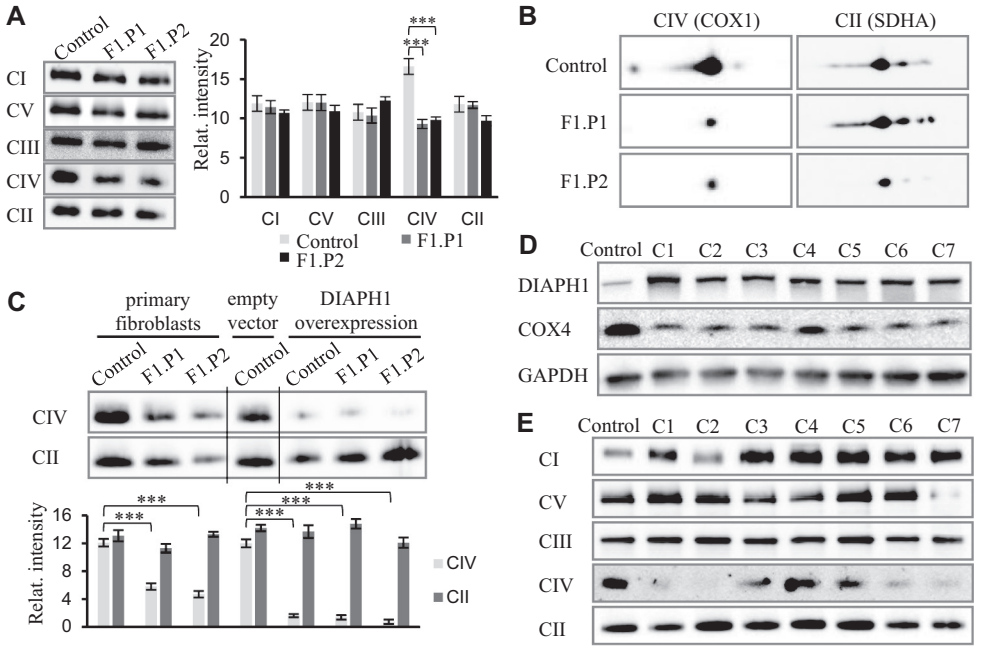

FIG 4. DIAPH1 affects CIV abundance. **A,** BN-PAGE for mitochondrial respiratory complexes indicated selective deficiency of CIV in patient-derived immortalized fibroblasts. **B,** 2D-SDS-PAGE querying amount of CIV (COX1 staining) and complex II (CII, SDHA staining) in patient and control fibroblasts. WT-*DIAPH1* expression construct was introduced to patient and healthy control–derived immortalized fibroblasts, and expression of several proteins and respiratory complexes was queried by western blotting in (**C**) BN-PAGE for CIV and CII. **D,** SDS-PAGE for DIAPH1 and COX4 (CIV subunit) in individual WT-*DIAPH1*-expression clones; GAPDH was used as a loading control. **E,** BN-PAGE for mitochondrial respiratory complexes in individual clones. Bars represent mean band intensity and error bars SD from 3 separate sample preparations. Vertical black lines indicate the lanes were run on the same gel but were noncontiguous. *BN-PAGE*, Blue Native Polyacrylamide Gel Electrophoresis; *Relat.*, relative. *P* values were calculated using Student *t* test: $*P < .05$, $**P < .01$, $***P < .001$.

donor PBMCs reproduced the T-cell activation defect detected in patients lacking *DIAPH1*.

T cells from patients with SCBMS exhibit impaired cytoskeletal regulation

To investigate whether the mechanism of the T-cell activation defect was related to the role of *DIAPH1* in regulation of the cytoskeleton, we studied cell morphology and adhesion, as well as F-actin and α-tubulin organization by immunofluorescence staining and microscopic imaging of T cells from patients and healthy donors. When seeded on CD3/CD28 antibody–coated surface, fewer patient than control cells were able to adhere (Fig 3, *A*). In addition, patient cells seemed more circular than control cells (Fig 3, *B* and *C*). Measurement of the MTOC distance from surface in T cells seeded on ICAM-1 and CD3 antibody–coated wells indicated less efficient MTOC reorientation to the immunologic synapse in patient-derived T cells than control cells (Fig 3, *D* and *E*). These results suggest altered cytoskeletal regulation in T cells lacking *DIAPH1*. No consistent changes were found in amount or localization of F-actin or mitochondria. We also tested chemotaxis of T cells cultured for 10 days after stimulation with soluble CD3/CD28 antibodies, but found no difference in SDF1-α–driven chemotaxis between patients (F2.P3 and F4.P5) and controls (see Fig E8 in this article's Online Repository at www.jacionline.org).

DIAPH1 regulates mitochondrial respiration through complex IV

In F1 patient–derived immortalized fibroblasts, we examined the levels of mitochondrial respiratory chain complexes of the mitochondrial oxidative phosphorylation system. Blue Native Polyacrylamide Gel Electrophoresis analysis for complexes I to V (CI-CV) revealed isolated deficiency of complex IV (CIV) (Fig 4, *A* and *B*). To confirm the link between *DIAPH1* and CIV by complementation, we introduced a full-length WT-*DIAPH1* expression construct into immortalized patient and control fibroblasts by lentiviral gene transfer. Surprisingly, instead of normalizing the amount of fully assembled CIV, *DIAPH1* overexpression resulted in a dramatic decrease in CIV amount in both control and patient total cell pools (Fig 4, *C*). In addition, overexpression of *DIAPH1* led to a decrease in actin levels (see Fig E9 in this article's Online Repository at www.jacionline.org). On examination of individual patient fibroblast overexpression clones, all clones showed higher *DIAPH1* expression than WT fibroblasts (Fig 4, *D*). The expression of COXIV (an individual subunit of complex IV) and the amount of fully assembled CIV varied among separate clones expressing WT-*DIAPH1* (Fig 4, *D* and *E*). One of the clones (C4) had reached the normal amount of fully assembled complex IV after the complementation and thus the CIV defect was rescued by the expression of WT-*DIAPH1*. Altogether this finding confirms that the CIV deficiency detected in patient fibroblasts originally was due to the lack of normal expression of *DIAPH1*.

By immunocytochemistry, we studied the distribution of the mitochondrial network in the immortalized fibroblasts using antibodies against Tom20, a mitochondrial outer membrane protein, and MT-CO1, a subunit of complex IV (see Fig E10 in this article's Online Repository at www.jacionline.org). Staining for DIAPH1 showed a lack of DIAPH1 in patient fibroblasts and clear overexpression of the protein after the complementation in both patient and control fibroblasts. In WT cells, most of the DIAPH1 protein localized to the cytoplasm and there was no colocalization with mitochondrial markers. Interestingly, in patient-derived fibroblasts overexpressing WT-*DIAPH1*, MT-CO1 had a strong perinuclear localization, but based on staining for Tom20, the overall distribution of the mitochondrial network was not changed.

Mitochondrial function in T cells lacking DIAPH1

Because we had detected reduced CIV in patient fibroblasts, we hypothesized that the immunodeficiency in patients with SCBMS could also be linked to altered mitochondrial function. Hence, we analyzed mitochondrial membrane potential (MMP) of patient- and control-derived lymphocytes by treating the cells with tetramethylrhodamine ethyl ester, a dye that accumulates in mitochondria, based on their negative MMP. Although results from $CD4^+$ cells were comparable between patients and controls, the tetramethylrhodamine ethyl ester signal-profile differed markedly between control and patient $CD8^+$ T cells (see Fig E11, *A*, in this article's Online Repository at www.jacionline.org). In control $CD3^+CD8^+$ cells, 2 populations with different peak fluorescence intensities were detected, whereas patient (F2.P3 and F3.P4) $CD3^+CD8^+$ cells showed only 1 population with an MMP signal localizing between those of the populations detected in controls.

To investigate whether there were differences in mitochondrial mass between samples, lymphocytes were stained with nonylacridine orange, a reagent that enters mitochondria independently of MMP. Patients, especially F2.P3, had a higher number of lymphocytes with a slightly lower mitochondrial mass (Fig E11, *B*).

We also assayed upregulation of cellular and mitochondrial calcium after activation with anti-CD3/CD28 beads in PBLs loaded with the fluorescent Ca^{2+} indicators Fluo-4 AM and Rhod-2 AM, respectively. To account for differences in reagent loading between samples, we analyzed signal intensity fold induction in response to stimulation. Patient PBLs exhibited a significantly weaker upregulation of mitochondrial Ca^{2+} in response to stimulation than controls (Fig E11, *C*).

DISCUSSION

In 5 patients from 4 unrelated Finnish pedigrees, we found homozygosity for a rare *DIAPH1* splice variant (c.684+1G>A) that leads to SCBMS via loss of the DIAPH1 protein. This variant is enriched in the Finnish population at an allele frequency of roughly 0.1%, and haplotype analysis implied a common ancestral origin for the variant. The *DIAPH1* c.684+1G>A variant is responsible for all cases of SCBMS identified in Finland thus far and is, to our knowledge, the first disease-causing variant in *DIAPH1* to have population-level impact. In addition, 2 additional patients originating from Oman with no known relation to previously published patients were found homozygous for the *DIAPH1*:c.2769delT;p.F923fs variant.[22]

The SCBMS syndrome seems to be readily identifiable by the hallmark symptoms of microcephaly, early-onset refractory epileptic seizures, cortical blindness, and intellectual disability exhibited by all patients.[12,22] In addition, all patients reported here had findings supporting immunodeficiency and some had signs of mitochondrial dysfunction. Clinically, the patients suffered from infection susceptibility and B-cell lymphomas, both of which are common occurrences in immunodeficient patients.[35,36] Immunologic investigations revealed that the patients were severely deficient in naive T-cell populations. This implies that similar problems in T-cell egression from the thymus take place in patients with SCBMS as have been demonstrated in *DIAPH1*$^{-/-}$ mice.[14] Moreover, upregulation of activation markers and proliferation of patient T cells in response to stimulation by mitogens or anti-CD3/CD28 was markedly reduced similarly to what has been seen in the *DIAPH1*$^{-/-}$ mouse model.[9,14] This defect was reproduced by CRISPR-Cas9 knockout of *DIAPH1* in healthy donor PBMCs, indicating that depressed T-cell immunity in patients is directly caused by lack of *DIAPH1*. Variation in the severity of the T-cell activation defect between patients and between healthy donor cells subjected to CRISPR-Cas9 knockdown of *DIAPH1* suggests modifying genetic factors.

While investigating the mechanism behind the functional T-cell defect, we found that patient-derived T cells exhibited impaired adhesion and inefficient MTOC translocation to the immunologic synapse. This cytoskeletal reorganization is essential for T-cell function.[37] An MTOC repolarization defect has also been demonstrated previously in a Jurkat *DIAPH1* knockdown model.[15] Considering these and previously published results on functions of DIAPH1 in actin nucleation and microtubule organization, immune presentations in patients with SCBMS are not surprising, because mutations in several genes involved in regulation of the cytoskeleton cause primary immunodeficiency.[38]

DIAPH1 has previously been demonstrated to regulate mitochondrial motility and distribution.[6,7] However, the mitochondrial network in SCBMS patient–derived fibroblasts seemed normal based on Tom20 staining. Instead, these cells showed deficiency of CIV, an integral part of mitochondrial respiration and regulator of mitochondrial oxidative phosphorylation.[39] CIV deficiency is one of the most common mitochondrial diseases and can be caused by mutations in several genes encoding for CIV subunits or assembly factors.[40] Typical pathology is somewhat dependent on the affected genes and tissues, but invariably includes encephalopathy, which is also a significant symptom of SCBMS. In patient T cells, we found changes in mitochondrial membrane potential and calcium. Changes in MMP in patient's $CD8^+$ cells could reflect alterations in $CD8^+$ naive to experienced cell ratio, mitochondrial energy production, or both.[41,42] Patient PBL also showed attenuated elevation of mitochondrial calcium in response to T-cell receptor engagement. This could be secondary to impairment of MTOC localization, because activation of calcium influx at the immunologic synapse is dependent on cytoskeletal reorganization.[43] Because, however, mitochondrial localization and bioenergetics are a major regulator of immune cell function,[44-48] immunometabolism in patients with SCMBS would be an interesting target for future investigations.

Conclusions

Our observations suggest that biallelic loss of *DIAPH1* negatively affects T-cell function and can lead to combined immunodeficiency. Hence, clinicians treating patients with SCBMS should be aware of a heightened risk for developing severe or recurrent infections and lymphoma. Furthermore, our findings indicate that the pathogenetic mechanism of SCBMS may be linked to impaired regulation of cytoskeletal organization and to mitochondrial dysfunction. However, the exact mechanistic links between *DIAPH1* and the cytoskeleton, mitochondrial function, CIV, and T-cell responses warrant further investigations.

We thank Riitta Herva (Oulu University Hospital) for her contributions to this study, FIMM Technology Centre Sequencing Unit for NGS library preparation and sequencing, Biocenter Finland High Content Imaging and Analysis Core Unit and High Throughput Biomedicine Unit at FIMM, HiLIFE, UH for immunostainings and microscopy, and Biocenter Finland, Biocenter Oulu Light Microscopy Core Facility, Biocenter Oulu Virus Core Facility, THL Biobank Laboratory (Helsinki, Finland), and Markus Vähä-Koskela (FIMM), Pirjo Keränen (University of Oulu), and Artem Kalinichenko (Ludwig Boltzmann Institute for Rare and Undiagnosed Diseases) for their technical assistance in execution of experiments.

Key messages

- **Clinicians treating patients with SCBMS should be aware of a higher risk for persistent infections and lymphoma.**
- **Loss of *DIAPH1* can result in aberrant B- and T-cell maturation and reduction in T-cell functionality due to defects in cytoskeletal organization.**
- **Mitochondrial dysfunction may underlie aspects of *DIAPH1*-related disease.**

REFERENCES

1. Watanabe N, Madaule P, Reid T, Ishizaki T, Watanabe G, Kakizuka A, et al. p140mDia, a mammalian homolog of *Drosophila diaphanous*, is a target protein for Rho small GTPase and is a ligand for profilin. EMBO J 1997;16:3044-56.
2. Palazzo A, Cook T, Alberts A, Gundersen G. mDia mediates Rho-regulated formation and orientation of stable microtubules. Nat Cell Biol 2001;3:723-9.
3. Watanabe N, Kato T, Fujita A, Ishizaki T, Narumiya S. Cooperation between mDia1 and ROCK in Rho-induced actin reorganization. Nat Cell Biol 1999;1:136-43.
4. Machaidze G, Sokoll A, Shimada A, Lustig A, Mazur A, Wittinghofer A, et al. Actin filament bundling and different nucleating effects of mouse diaphanous-related formin FH2 domains on actin/ADF and actin/cofilin complexes. J Mol Biol 2010;403:529-45.
5. Campellone KG, Welch MD. A nucleator arms race: cellular control of actin assembly. Nat Rev Mol Cell Biol 2010;11:237-51.
6. Li D, Sewer MB. RhoA and DIAPH1 mediate adrenocorticotropin-stimulated cortisol biosynthesis by regulating mitochondrial trafficking. Endocrinology 2010;151:4313-23.
7. Minin A, Kulik A, Gyoeva F, Li Y, Goshima G, Gelfand V. Regulation of mitochondria distribution by RhoA and formins. J Cell Sci 2006;119:659-70.
8. Galbraith KK, Kengaku M. Multiple roles of the actin and microtubule-regulating formins in the developing brain. Neurosci Res 2019;138:59-69.
9. Eisenmann KM, West RA, Hildebrand D, Kitchen SM, Peng J, Sigler R, et al. T cell responses in mammalian diaphanous-related formin mDia1 knock-out mice. J Biol Chem 2007;282:25152-8.
10. Tanizaki H, Egawa G, Inaba K, Honda T, Nakajima S, Moniaga CS, et al. Rho-mDia1 pathway is required for adhesion, migration, and T-cell stimulation in dendritic cells. Blood 2010;116:5875-84.
11. Shi Y, Zhang J, Mullin M, Doug B, Alberts AS, Siminovitch KA. The mDial formin is required for neutrophil polarization, migration, and activation of the LARG/RhoA/ROCK signaling axis during chemotaxis. J Immunol 2009;182:3837-45.
12. Ercan-Sencicek AG, Jambi S, Franjic D, Nishimura S, Li M, El-Fishawy P, et al. Homozygous loss of DIAPH1 is a novel cause of microcephaly in humans. Eur J Human Genet 2015;23:165-72.
13. Thumkeo D, Shinohara R, Watanabe K, Takebayashi H, Toyoda Y, Tohyama K, et al. Deficiency of mDia, an actin nucleator, disrupts integrity of neuroepithelium and causes periventricular dysplasia. Plos One 2011;6:e25465.
14. Sakata D, Taniguchi H, Yasuda S, Adachi-Morishima A, Hamazaki Y, Nakayama R, et al. Impaired T lymphocyte trafficking in mice deficient in an actin-nucleating protein, mDia1. J Exp Med 2007;204:2031-8.
15. Gomez TS, Kumar K, Mecleiros RB, Shimizu Y, Leibson PJ, Billadeau DD. Formins regulate the actin-related protein 2/3 complex-independent polarization of the centrosome to the immunological synapse. Immunity 2007;26:177-90.
16. Peng J, Kitchen SM, West RA, Sigler R, Eisenmann KM, Alberts AS. Myeloproliferative defects following targeting of the Drf1 gene encoding the mammalian diaphanous-related formin mDia1. Cancer Res 2007;67:7565-71.
17. Narumiya S, Tanji M, Ishizaki T. Rho signaling, ROCK and mDia1, in transformation, metastasis and invasion. Cancer Metastasis Rev 2009;28:65-76.
18. Eisenmann KM, Dykema KJ, Matheson SF, Kent NF, DeWard AD, West RA, et al. 5q-myelodysplastic syndromes: chromosome 5q genes direct a tumor-suppression network sensing actin dynamics. Oncogene 2009;28:3429-41.
19. Lynch E, Lee M, Morrow J, Welcsh P, Leon P, King M. Nonsyndromic deafness DFNA1 associated with mutation of a human homolog of the Drosophila gene diaphanous. Science 1997;278:1315-8.
20. Ueyama T, Ninoyu Y, Nishio S, Miyoshi T, Torii H, Nishimura K, et al. Constitutive activation of DIA1 (DIAPH1) via C-terminal truncation causes human sensorineural hearing loss. Embo Mol Med 2016;8:1310-24.
21. Stritt S, Nurden P, Turro E, Greene D, Jansen SB, Westbury SK, et al. A gain-of-function variant in DIAPH1 causes dominant macrothrombocytopenia and hearing loss. Blood 2016;127:2903-14.
22. Al-Maawali A, Barry BJ, Rajab A, El-Quessny M, Seman A, Coury SN, et al. Novel loss-of-function variants in DIAPH1 associated with syndromic microcephaly, blindness, and early onset seizures. Am J Med Genet Part A 2016;170:435-40.
23. Yao J, Shoubridge E. Expression and functional analysis of SURF1 in Leigh syndrome patients with cytochrome c oxidase deficiency. Hum Mol Genet 1999;8:2541-9.
24. Weraarpachai W, Antonicka H, Sasarman F, Seeger J, Schrank B, Kolesar JE, et al. Mutation in TACO1, encoding a translational activator of COX I, results in cytochrome c oxidase deficiency and late-onset Leigh syndrome. Nat Genet 2009;41,833-U96.
25. Haapaniemi EM, Kaustio M, Rajala HLM, van Adrichem AJ, Kainulainen L, Glumoff V, et al. Autoimmunity, hypogammaglobulinemia, lymphoproliferation, and mycobacterial disease in patients with activating mutations in STAT3. Blood 2015;125:639-48.
26. Stone KD, Feldman HA, Huisman C, Howlett C, Jabara HH, Bonilla FA. Analysis of in vitro lymphocyte proliferation as a screening tool for cellular immunodeficiency. Clin Immunol 2009;131:41-9.
27. Schindelin J, Arganda-Carreras I, Frise E, Kaynig V, Longair M, Pietzsch T, et al. Fiji: an open-source platform for biological-image analysis. Nat Methods 2012;9:676-82.
28. Wickham H. ggplot2: Elegant graphics for data analysis. Springer-Verlag New York; 2016. ISBN 978-3-319-24277-4, https://ggplot2.tidyverse.org.
29. RStudio Team. RStudio: integrated development for R. Boston, MA: Rstudio. 2020. Available at: http://www.rstudio.com/.
30. Karczewski KJ, Francioli LC, Tiao G, Cummings BB, Alföldi J, Wang Q, et al. Variation across 141,456 human exomes and genomes reveals the spectrum of loss-of-function intolerance across human protein-coding genes [published online ahead of print January 30, 2019]. bioRxiv. https://doi.org/10.1101/531210.
31. Kaprio J. The Finnish Twin Cohort Study: an update. Twin Res Hum Genet 2013;16:157-62.
32. Vartiainen E, Seppala T, Lillsunde P, Puska P. Validation of self reported smoking by serum cotinine measurement in a community-based study. J Epidemiol Community Health 2002;56:167-70.
33. Gandolfo LC, Bahlo M, Speed TP. Dating rare mutations from small samples with dense marker data. Genetics 2014;197:1315-U437.
34. Hautala TJ, Perelygina L, Vuorinen T, Hautala NM, Hagg PM, Bode MK, et al. Nitazoxanide may modify the course of progressive multifocal leukoencephalopathy. J Clin Immunol 2018;38:4-6.
35. Bin Riaz I, Faridi W, Patnaik MM, Abraham RS. A systematic review on predisposition to lymphoid (B and T cell) neoplasias in patients with primary

immunodeficiencies and immune dysregulatory disorders (inborn errors of immunity). Front Immunol 2019;10:777.
36. Tangye SG, Al-Herz W, Bousfiha A, Chatila T, Cunningham-Rundles C, Etzioni A, et al. Human inborn errors of immunity: 2019 Update on the Classification from the International Union of Immunological Societies Expert Committee. J Clin Immunol 2020;40:24-64.
37. Kloc M, Kubiak JZ, Li XC, Ghobrial RM. The newly found functions of MTOC in immunological response. J Leukoc Biol 2014; 95:417-30.
38. Janssen E, Geha RS. Primary immunodeficiencies caused by mutations in actin regulatory proteins. Immunol Rev 2019;287:121-34.
39. Pierron D, Wildman DE, Huettemann M, Markondapatnaikuni GC, Aras S, Grossman LI. Cytochrome c oxidase: evolution of control via nuclear subunit addition. Biochim Biophys Acta 2012;1817:590-7.
40. Diaz F. Cytochrome c oxidase deficiency: patients and animal models. Biochim Biophys Acta 2010;1802:100-10.
41. Sukumar M, Liu J, Mehta GU, Patel SJ, Roychoudhuri R, Crompton JG, et al. Mitochondrial membrane potential identifies cells with enhanced stemness for cellular therapy. Cell Metab 2016;23:63-76.
42. Li Y, Park J, Deng J, Bai Y. Cytochrome c oxidase subunit IV is essential for assembly and respiratory function of the enzyme complex. J Bioenerg Biomembr 2006;38:283-91.
43. Joseph N, Reicher B, Barda-Saad M. The calcium feedback loop and T cell activation: how cytoskeleton networks control intracellular calcium flux. Biochim Biophys Acta 2014;1838:557-68.
44. Angajala A, Lim S, Phillips JB, Kim J, Yates C, You Z, et al. Diverse roles of mitochondria in immune responses: novel insights into immuno-metabolism. Front Immunol 2018;9:1605.
45. Kapniciz SM, Pacheco SE, McGuire PJ. The emerging role of immune dysfunction in mitochondrial diseases as a paradigm for understanding immunometabolism. Metabolism Clin Exp 2018;81:97-112.
46. Alosaimi MF, Shendi H, Beano A, Stafstrom K, El Hawary R, Meshaal S, et al. T-cell mitochondrial dysfunction and lymphopenia in DOCK2-deficient patients. J Allergy Clin Immunol 2019;144:306.
47. Mehta MM, Weinberg SE, Chandel NS. Mitochondrial control of immunity: beyond ATP. Nat Rev Immunol 2017;17:608-20.
48. Quintana A, Schwindling C, Wenning AS, Becherer U, Rettig J, Schwarz EC, et al. T cell activation requires mitochondrial translocation to the immunological synapse. Proc Natl Acad Sci U S A 2007;104:14418-23.